




Synchrotron x-Ray Study of Heterostructured Materials: A Review

JIE YAN,¹ WEIXIA DONG,² PEIJIAN SHI,¹ TIANYI LI,³
WENJUN LIU,³ YAN-DONG WANG,⁴ XUN-LI WANG,^{2,5}
YUNTIAN ZHU ^{1,6} and YANG REN^{2,7}

1.—Department of Materials Science and Engineering, City University of Hong Kong, Kowloon, Hong Kong, China. 2.—Department of Physics, City University of Hong Kong, Kowloon, Hong Kong, China. 3.—X-Ray Science Division, Advanced Photon Source, Argonne National Laboratory, Lemont, IL 60439, USA. 4.—Beijing Advanced Innovation Center for Materials Genome Engineering, State Key Laboratory for Advanced Metals and Materials, University of Science and Technology Beijing, Beijing 100083, China. 5.—Center for Neutron Scattering, City University of Hong Kong Shenzhen Research Institute, Shenzhen 518057, China. 6.—e-mail: y.zhu@cityu.edu.hk. 7.—e-mail: yangren@cityu.edu.hk

Heterostructured materials (HSMs) have shown great potential for breaking the strength-ductility tradeoff. HSMs consist of heterogeneous zones that may have different sizes, shapes, compositions, structures, etc. Interactions and competitions among them often lead to unprecedented properties. However, due to the complex structures in a broad range of length scales, it is challenging to unravel deformation physics and strengthening mechanisms underlying extraordinary mechanical properties. Synchrotron x-rays provide powerful techniques and indispensable tools for investigating HSMs at various length scales. Here, we will present *in situ* high-energy x-ray diffraction and Laue x-ray microdiffraction techniques and their application in studying the HSMs. The principles of these techniques will be briefly introduced. We will focus on their application in studying stress partitioning and plastic accommodation during tensile deformation, thermo-driven and/or stress-driven phase transformations and various deformation microstructures like geometrically necessary dislocations and local stress/strain distributions, etc., in HSMs. Some important findings will be summarized. Challenging issues remain in studying HSMs and will be discussed.

INTRODUCTION

Strong and ductile structural materials are desired for safety and energy conservation.¹ Achieving an excellent strength-ductility combination among conventional homogeneous materials is challenging, as a gain in strength often comes with a sacrifice of ductility, giving rise to a strength-ductility tradeoff.² As a new class of structural materials, however, heterostructured materials (HSMs)^{3–5} have shown great potential for tackling this issue.

The mechanical properties of HSMs are determined by their heterogeneous microstructures. Under mechanical loads, strong mechanical interactions and competitions are generated among the heterogeneous zones because of the existing microstructure heterogeneity, which may provide various types of enhanced mechanical properties, including tensile strength and uniform elongation,^{4,6–8} fracture toughness,^{9–11} creep resistance,^{12,13} super plasticity,^{14,15} and fatigue properties.^{16,17} Specifically, a typical HSM may consist of heterogeneous zones with dramatically different strengths (> 100%).³ During tensile deformation, the back stress first generated in soft zones is believed to help with the development of the forward stress in hard zones, which together

(Received November 24, 2022; accepted January 16, 2023;
published online February 23, 2023)

produce the hetero-deformation induced (HDI) stress. By matching the strength of the heterogeneous zones and creating strong zone interfaces, the interaction between the back and forward stress can contribute to a simultaneous increase in strength and ductility.^{5,18} Although a superior strength-ductility combination has been achieved in the newly developed materials, fundamental knowledge about their deformation physics and strengthening mechanisms underlying the extraordinary mechanical property is still sparse.⁵

Characterizing the evolution of local stress/strain during deformation is critical to unraveling the deformation physics but remains technically challenging. Although significant progress has already been made by using the methods of digital image correlation (DIC) and electron backscatter diffraction (EBSD),^{19,20} the popular surface measurements have their limitations because the deformation characteristics of the subsurface are often different from the surface because of a triaxial stress state inside the bulk material. Moreover, because the local deformation behavior directly relies on the nearby microstructures, the local stress/strain analysis based on these measurements is further complicated by the heterostructures in materials.²¹ To study the heterogeneous deformation of HSMs experimentally, the distribution of microstructural heterogeneities should be controlled systematically so that a unified model to describe the mechanical interactions and competitions may well be developed.

Compared with surface measurements, synchrotron-based x-ray methods can be employed to study deformation in three dimensions, including the overall deformation of bulky samples of millimeter thick and the local heterogeneous deformation at a micron/submicron level. Currently, the synchrotron x-ray study of micromechanical behavior has been extensively performed in different metallic materials, and many interesting findings have been reported in the literature.^{8,10,14,15,18,21–38} Combining in situ straining and/or thermal processes, researchers can characterize lattice stress/strain partitioning behavior and interphase stress,^{10,18,23,29,33} calculate residual stress,^{24,32,38} and investigate microstructure evolution and phase transformations.^{15,22,31,34–37}

This article briefly reviews the synchrotron x-ray study of heterostructured materials, with the focus being on the characterization of deformation microstructures and, based on this, the current progress in understanding deformation mechanisms and phase transformations. First, in situ high-energy x-ray diffraction (HEXRD) and Laue x-ray microdiffraction techniques are introduced. Then, typical outcomes obtained by using these techniques are reviewed with the purpose of demonstrating their capability of studying plastic deformation and phase transformations in HSMs. Finally, the current challenges of characterizing the evolution of

strain by synchrotron XRD measurements are presented, and the new directions that are valuable for further study are discussed.

PRINCIPLES OF SYNCHROTRON XRD AND GENERAL EXPERIMENTAL PROCEDURES

High-Energy x-Ray Diffraction

The characteristics of synchrotron x-ray diffraction are its high energy and high flux. The volume of a sample scattered in a test is normally determined by its beam energy and size. The beam size is usually adjustable, depending on the requirements of a specific experiment. Generally, for high-energy x-ray experiments, the energy range of x-ray photons generated by synchrotron radiation is between 50 keV and 150 keV, corresponding to an x-ray wavelength between 0.25 Å and 0.08 Å. Thus, the wavelength is significantly smaller than the interplanar spacing having low Miller indices. This brings about a diffraction geometry quite similar to that in a transmission electron microscope, with Bragg angles that satisfy the diffraction condition being very small, normally just several degrees.²⁹ This has considerably facilitated in situ XRD measurements under complex sample environments that are difficult for conventional XRD.³⁹ Another advantage of x-rays with small wavelengths is that they can cover large reciprocal space, which is critical for total scattering experiments.⁴⁰

The diffraction geometry of in situ HEXRD is shown in Fig. 1. The incident beam passes through the slits with the beam size desired and then hits a sample to generate diffraction signals. The direct beam will be blocked by a beam stop. A 2D detector behind the beam stop is used to record the diffracted x-rays. The advantage of using 2D detectors is that they can collect the full diffraction pattern within a scattering cone, which not only significantly expedites the data collection time but also directly helps visualize the texture of a sample, if there is any. To obtain a series of images with high quality diffraction data during in situ straining and/or thermal process, experimenters need to adjust the exposure time according to the maximum intensity of the diffraction image, consequently making it feasible to refine and analyze the diffraction peaks and then to calculate the overall lattice stress in the sample.

Wide and Small Angle x-Ray Scattering Measurements

Wide and small angle x-ray scattering (WAXS/SAXS) measurements can be conducted simultaneously by adding a setup for the SAXS measurement to the HEXRD. A geometry of this technique is illustrated in Fig. 2. It operates with the transmission mode by leaving a narrow opening at the center of WAXS detectors. Generally, WAXS signals are obtained at Bragg angles $2^\circ < 2\theta < 20^\circ$, while SAXS

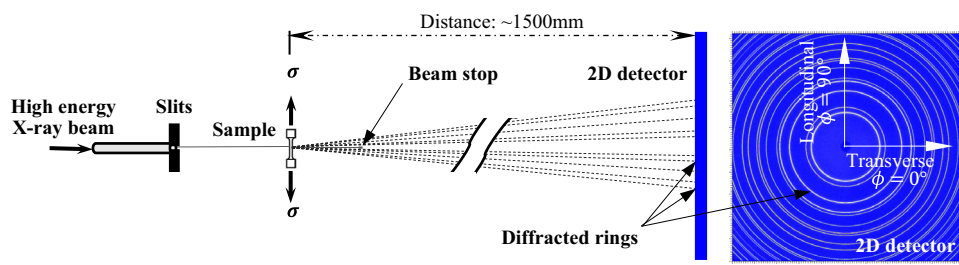


Fig. 1. Schematic illustration of the experimental set-up for in-situ loading HEXRD.

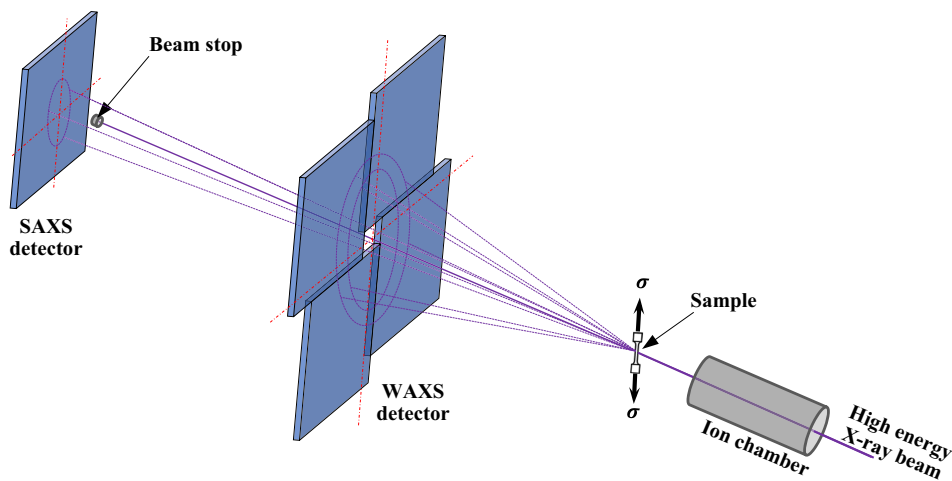


Fig. 2. Schematic illustration of wide and small angle x-ray scattering measurements.

at $2\theta < 1^\circ$.⁴¹ Patterns recorded on the WAXS 2D detector can be converted to line profiles and then used to calculate the relative peak shift and broadening. However, the 2D patterns can also be used for texture analysis if there is any. SAXS signals are sensitive to nanoscale electron density differences between matrices and particles or voids.⁴¹ Thus, data collected on the SAXS detector can be processed to analyze nano-precipitation behavior, nanoscale heterostructures, and nano-particle size distribution in materials or to understand void formation and evolution during plastic deformation at the necking stage.

Laue x-ray Microdiffraction in 3D

Synchrotron-based Laue x-ray microdiffraction, developed for the last 2 decades, has become an effective tool for characterizing samples at micron and submicron scales. Laue x-ray microdiffraction can be applied to measure and analyze local deformation.^{21,42} Compared with in situ surface measurements like EBSD and DIC, a distinctive feature of the in situ microdiffraction is the full capability of characterizing deformation along the depth direction with an even higher spatial resolution. Thus, this characterization method can satisfy the essential requirement of determining the three-dimensional deformation microstructures in materials and the dynamic evolution of the local stress/strain,

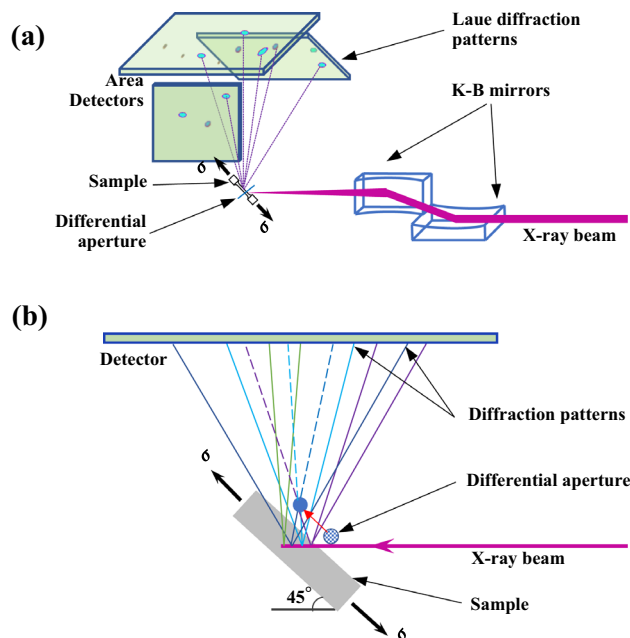


Fig. 3. (a) Setup of Laue x-ray microdiffraction. (b) Schematic illustration of the diffraction geometry.

especially during in situ loading experiments. Since the heterogeneous deformation in HSMs exists ubiquitously at the sub-micron level,⁵ such a

capability can indubitably play a key role in studying their deformation mechanism.

Figure 3 shows the diffraction geometry of Laue x-ray microdiffraction. A polychromatic or monochromatic x-ray microbeam with high flux is used to probe the sample (see Fig. 3a). In contrast to the HEXRD measurement in x-ray transmission mode, Laue microdiffraction works in the Bragg reflection mode.⁴³ Additionally, the x-ray beam size, typically $< 0.5 \mu\text{m} \times 0.5 \mu\text{m}$ achieved by a pair of K-B focusing mirrors, is significantly smaller than that of HEXRD measurements. However, this ultra-bright microbeam can still penetrate the crystal samples (e.g., steel) with a depth distance up to a hundred microns, meaning that the deformation microstructures deep into the sample can be examined.

Details of the microdiffraction in 3D are shown in Fig. 3b. Geometrically, the microbeam hits the sample surface at 45 degrees, and the detector on the top of the sample records the Laue diffraction patterns. A platinum wire, moving near the sample surface, serves as a differential aperture for depth profiling, with a depth resolution of typically about $1 \mu\text{m}$. Thus, a large sample volume of interest can be scanned by moving the sample stage step-by-step and then repeating the depth measurements with differential aperture. By using this technique, the diffraction information of a volume can be measured with a spatial resolution as high as $0.5 \mu\text{m} \times 0.5 \mu\text{m} \times 1.0 \mu\text{m}$, and the local distributions of elastic lattice strains inside a large volume can be quantitatively measured with an accuracy of 1×10^{-4} .²¹

This method is particularly useful in measuring the deformation structure of heterostructured layered samples.⁴⁴ With different microstructures repeated regularly from the surface to the interior, the layered structure is particularly suitable for the investigation of heterogeneous deformation in HSMs. In situ microdiffraction using monochromatic and polychromatic beams can be used to measure the local strain evolution of different layers under tensile loading.

Experimental Procedures and Data Processing

After the equipment is set up, a test of a reference sample, like CeO_2 , is first carried out to examine whether the equipment works correctly and also for calibration.²⁹ The result can be fitted by using various software to obtain calibration parameters, such as the beam center, detector tilt, sample-to-detector distance, etc., which will be applied to data treatments and analysis under the same experimental condition. The general procedures for processing data and calculating lattice strains show below:

1. The collected diffraction patterns on a 2D detector are converted from polar to Cartesian

coordinates in N radial $\times M$ azimuthal bins. For selected crystallographic reflections, the profile of the peak intensity as a function of radial distance is fitted using a pseudo-Voigt function to find the average center of the peak intensity (R) together with the full width at half maximum (FWHM) values of the diffraction peaks.

2. The interplanar spacing (d^{hkl}) concerned is determined by using Bragg's law:

$$\lambda = 2d^{\text{hkl}} \sin(\theta^{\text{hkl}}) \quad (1)$$

where θ^{hkl} is the Bragg angle. The lattice strain, ε^{hkl} , is then determined by:²³

$$\varepsilon^{\text{hkl}} = (d^{\text{hkl}} - d_0^{\text{hkl}}) / d_0^{\text{hkl}} \quad (2)$$

where d_0^{hkl} and d^{hkl} are the interplanar spacings of the specific plane, (hkl), in a stress-free and stressed material, respectively. Note that the interplanar spacings calculated are assumed as the averaged values of all (hkl) planes measured along certain directions in the specimen.

3. For tensile loading, it is essential to determine two volume-averaged lattice strain components, i.e., ε_{11} and ε_{22} , which are parallel and perpendicular to the tensile axis, respectively. After all M azimuthal bins with an angle increment of $\Delta\varphi$ ($\Delta\varphi = 360^\circ/M$) are fitted, the peak intensity $R(\varphi)$ can be related to $\sin^2(\psi)$ for all applied stress, where $\varphi = k \bullet \Delta\varphi$ (k is an integer), and $\psi = \Delta\varphi + \theta \cos(\Delta\varphi)$, where θ is the Bragg angle.⁴⁵ Thus, the lattice strain at an angle related to the tensile axis for a given (hkl) reflection is calculated by:

$$\varepsilon(\varphi) = \frac{R_0 - R(\varphi)}{R_0} \quad (3)$$

where R_0 represents the peak intensity at the stress-free state. In this way, ε_{11} and ε_{22} equal to $\varepsilon(90^\circ)$ and $\varepsilon(0^\circ)$, respectively (see Fig. 1).

STUDYING HETEROGENEOUS DEFORMATION AND PHASE TRANSFORMATION BY HEXRD

Investigating Stress Partitioning and Strain Accommodation

The mutual accommodation between heterogeneous zones plays a key role in the excellent mechanical properties of HSMs. During deformation, these zones experience different deformation processes, which can be classified into elastic-elastic, elastoplastic, and plastic-plastic stages.³ Stress partitioning and load transfer take place between the heterogeneous zones at the beginning of the elastoplastic stage, and such typical heterogeneous

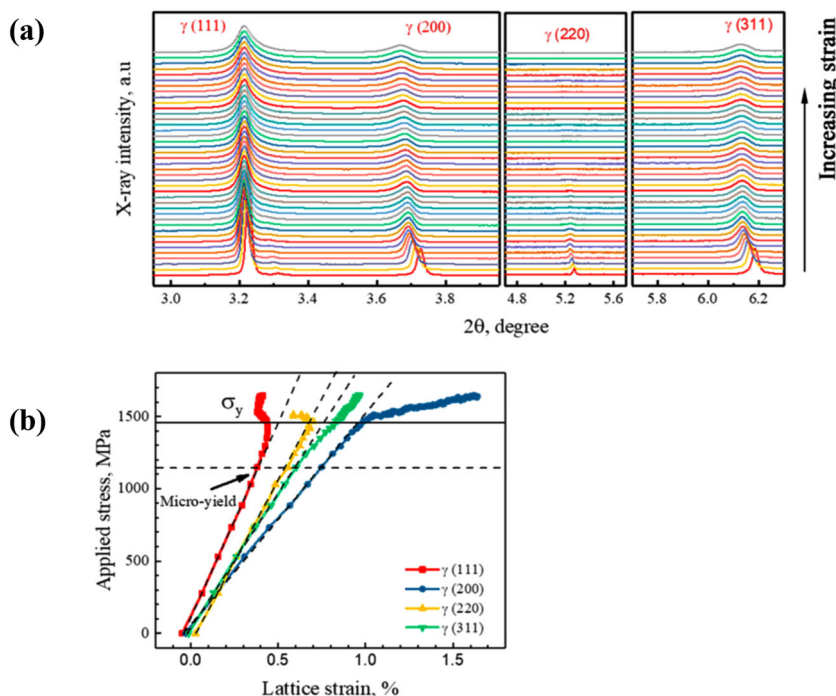


Fig. 4. Load partitioning of a high Mn steel with hetero-structures studied by *in-situ* HEXRD. (a) XRD spectrum in different crystal planes. (b) Applied stress vs lattice strain curves of different grain families. Yield stress σ_y is 1450 MPa, and micro-yielding occurs at stress of 1150 MPa. Reprinted with permission from Ref. 33, under the terms of the Creative Commons CC BY license.

deformation cannot be examined by traditional methods other than by using the *in situ* synchrotron HEXRD measurement.¹⁸

Findings of early studies on stress partitioning and load transfer by *in situ* HEXRD were reported in dual- and multi-phase steels, even though at that time, the concept of HSMs had not been developed.^{23,29,41} Using *in situ* HEXRD with tensile loading, Young et al.²³ measured the volume-averaged lattice elastic strains for various crystallographic planes of α -Fe and Fe_3C phases in an ultrahigh-carbon steel. A remarkable load transfer took place from the ductile α -Fe matrix to the elastic Fe_3C phase after the propagation of the Lüders band. Then, Cong et al.²⁹ studied the micromechanical behavior of ferrite/martensite dual-phase alloys, in which only a small difference existed in the phase crystallographic structures. In a word, measurement of stress or strain partitioning had been regarded as impossible before the advent of the *in situ* HEXRD or neutron diffraction technique.

Recently, the microscopic plastic response of a high Mn steel with heterostructures was investigated by *in situ* HEXRD³³ (see Fig. 4). The change of diffraction peaks and corresponding axial lattice strains with the applied stress can be clearly seen. It is interesting to find that the lattice strain of the (111) grain family began to deviate from linearity at a stress of 1150 MPa, which was much less than the macroscopic σ_y of 1450 MPa. This could be regarded as micro-yielding that happened at first in the (111) grain family, indicating an extended elastoplastic

stage inherent to materials with heterostructures.³ After global yielding, the rate of increase in lattice strain speeded up in (200) and (311) grain families, with the (200) grain family growing fastest and the (311) second. This trend was in sharp contrast to that of the (111) and (220) families, indicating load partitioning and load transfer between these grain families during plastic deformation.^{18,33} In short, the stress partition behavior of HSMs has been readily demonstrated by the *in situ* HEXRD technique.

The *in situ* HEXRD technique has also been used to elucidate how plastic accommodation evolves in heterostructured gradient materials. Wu et al.¹⁸ reported an alloy with a gradient structure consisting of the surface nano-structured (NS) layer and the central coarse-grained (CG) layer. During tensile loading, the gradient-structured alloy showed a layer-by-layer yielding phenomenon. Figure 5 shows the evolution of volume-averaged strain components, ε_{11} and ε_{22} , in the (110) grain family with the applied stress. The CG layer yielded first, and with micro-yielding initiation, plastic accommodation between the two layers started immediately (see ε_{11} in Fig. 5a). Load transfer from the CG layer to the NS layer is clearly shown, with the increase of elastic stress in the CG layer slowing down but that in the NS layer speeding up. In the transverse direction, an opposite trend for the evolution of elastic strain (ε_{22}) can be seen, which conforms to the Poisson effect. To determine the change in lattice strain of each layer, the authors

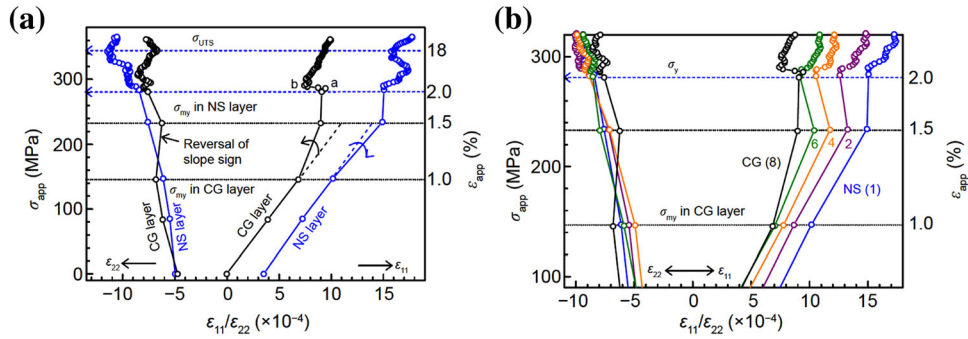


Fig. 5. Evolution of volume-averaged strain components, ϵ_{11} and ϵ_{22} , in (110) grain family with applied stress, (a) in both the NS and CG layers. (b) The gradual change in lattice strains from NS layer to CG layer. Reprinted with permission from Ref. 18.

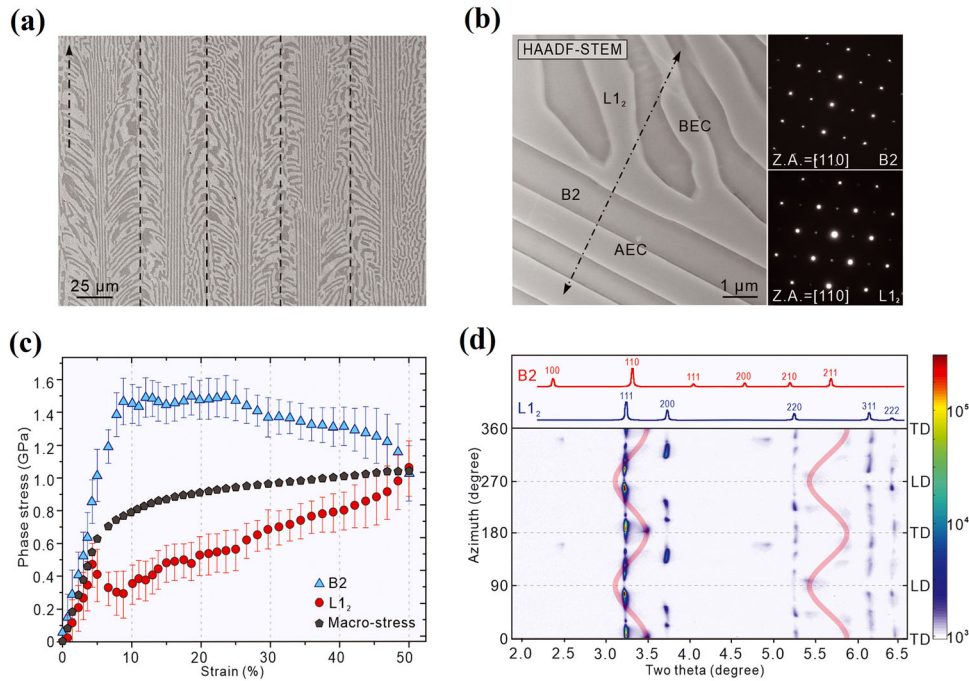


Fig. 6. (a) Hierarchically arranged herringbone microstructure. (b) HAADF-STEM image and related SAED patterns of B2 and L1₂ phases. (c) Real-time stress partitioning of B2 and L1₂ phases during tensile loading. (d) Selected 2D x-ray diffraction images along the full azimuthal angle (0° to 360°) at tensile strain of ~48%. Reprinted with permission from Ref. 10.

performed a layer-by-layer in situ HEXRD measurement from the NS layer to the CG layer (see NS (1) to CG (8) in Fig. 5b). A gradual change of slope from the NS layer to the CG layer represents a gradual elastoplastic transition, which can be regarded as evidence of strain accommodation during tensile loading in HSMs. However, the physical nature of the strain accommodation remains unclear and needs further investigation.

Recent years have witnessed great research interest in science communities in high entropy alloys (HEAs).^{10,34,46} The in situ HEXRD technique has also been used to investigate HEAs with heterostructures. For example, Shi et al.¹⁰ observed in an Al₁₉Fe₂₀Co₂₀Ni₄₁ eutectic HEA a real-time stress partitioning effect between B2 and L1₂ phases (see Fig. 6). The micro-yielding behavior of

the softer L1₂ phase led to stress relaxation and load transfer to the harder B2 phase, a phenomenon also seen in the gradient structure above (see Fig. 6c). After approaching a tensile strain of ~25%, however, the harder B2 phase began bearing less stress, but the softer L1₂ phase started carrying more stress thanks to the L1₂ phase's outstanding strain-hardening capability. This marks a gradual transfer of load from the hard but brittle B2 phase to the initially soft but gradually strain-hardened L1₂ phase. To exclude the possibility of strain-hardening that might be induced by conventional phase transformations, the authors also conducted 2D HEXRD diffraction investigations near the point of fracture. The result is shown in Fig. 6d. No newly transformed phase existed, while the diffraction lines of the B2 phase deviated severely from their

initial angle, showing the huge elastic strain stored in the B2 phase. In summary, the in situ HEXRD techniques enable researchers to obtain quantitative insights into the exceptional mechanical property of heterostructured materials.

Investigating Phase Transformations

The in situ HEXRD techniques have been applied to investigations of thermo- and/or stress-driven phase transformations in various materials.^{14,15,30,31,34} Thanks to the high-energy and high-flux x-ray beam, phase transformations of large samples with complicated phase constitutions can be studied under various testing conditions, including heating, cooling, and compressive and tensile loading treatments.

The micro-deformation behavior of a Nb/TiNi nanowire composite was investigated by in situ HEXRD during tensile deformation.¹⁴ This composite is a typical HSM with different crystal structures at the heterogeneous zones (see Fig. 7a). During tensile loading, the intensity of the B2-(211) diffraction peaks decreased gradually with increasing the global strain, meaning that the TiNi matrix (B2 structure) underwent a stress-induced martensitic transformation (B2 \rightarrow B19', see Fig. 7b and c). The crystallographic strain resulting from the martensitic transformation matched well with the theoretical limits of elastic strains of embedded nanomaterials, leading to effective load transfer from the TiNi matrix to the nanomaterials and consequently allowing them to achieve ultra-large elastic strains close to the theoretical limits. Thus, to obtain an effective load transfer from matrixes to nanophases, the crystallographic strain resulting from the transformations should match well with the theoretical limits of elastic strains of embedded nanophases. This result provides a strategy for designing materials with ultra-large elastic strains close to the theoretical limits.

The effect of temperatures on the precipitation and micromechanical behavior of HEAs has also

been investigated using thermal in situ HEXRD. For instance, Wang et al.³⁴ studied the phase structure evolution of $\text{Al}_{0.5}\text{Cr}_{0.9}\text{FeNi}_{2.5}\text{V}_{0.2}$ HEAs during in situ heating of the sample from 200 °C up to 1100 °C. The HEAs were pre-deformed to a thickness reduction of 72%, and the result is shown in Fig. 8. By raising the temperatures, the sequence of phase transformations shows FCC \rightarrow FCC + L1₂ + BCC \rightarrow FCC + L1₂ + BCC + B2 \rightarrow FCC + B2 \rightarrow FCC. Both precipitation and decomposition temperatures for L1₂ and BCC phases were clearly identified (see Fig. 8b and c). Pre-deformed conditions and subsequent heat treatments will also influence the precipitation behavior of alloys. Their results have shown that high-density defects induced by pre-deformation promoted the segregation of Cr and then facilitated the formation of coherent FCC/L1₂ spinodal nanostructure, resulting in an insignificant difference in phase stress between the FCC and the L1₂ phases. Thus, thermal in situ HEXRD provides us with a powerful tool for studying phase transformations of alloys with complex phase constitutions.

Analyzing Dislocation Evolution During Straining Process

Dislocation behavior is key to the plastic deformation of crystalline materials. In situ HEXRD has also been widely used to measure a sample's dislocation density during plastic deformation.^{47,48} Specifically, peak broadening quantified by the full width at half maximum (FWHM) of specific reflections is used to evaluate the evolution of dislocation density as a function of tensile strain. The modified William-Hall method is used for this calculation:⁸

$$\Delta K \cong \frac{0.9}{D} + \sqrt{\pi M^2 b^2 / 2} \cdot \sqrt{\rho} \cdot (KC^{0.5}) \quad (4)$$

where $K = 2\sin\theta/\lambda$; $\Delta K = 2\cos\theta(\Delta\theta)/\lambda$; θ and λ are the diffraction angle and the wavelength of x-rays, respectively; D , ρ , and b are the average grain or

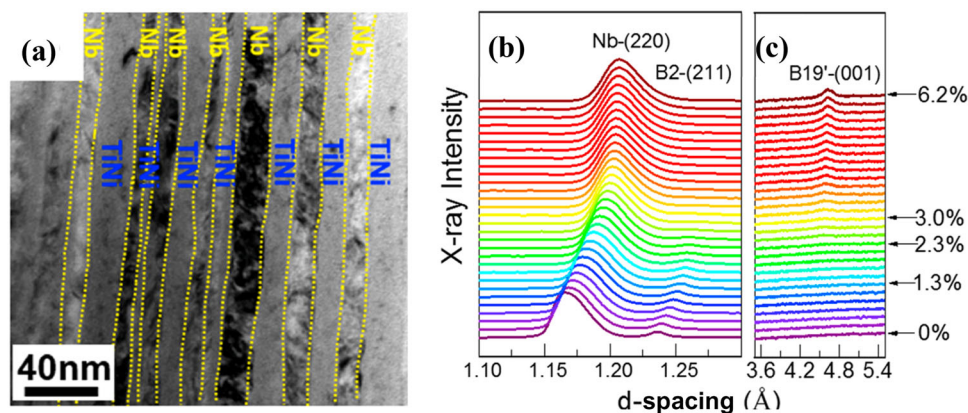


Fig. 7. Micro-deformation behavior of Nb/TiNi nano-lamellae composite. (a) TEM bright field image of multi-layered Nb/TiNi plate. (b) Evolution of the diffraction peaks of Nb-(220) and B2-(211) planes with loading. (c) 360°-integrated HEXRD patterns showing the evolution of B19'-(001) diffraction peak during tensile loading. Reprinted with permission from Ref. 14.

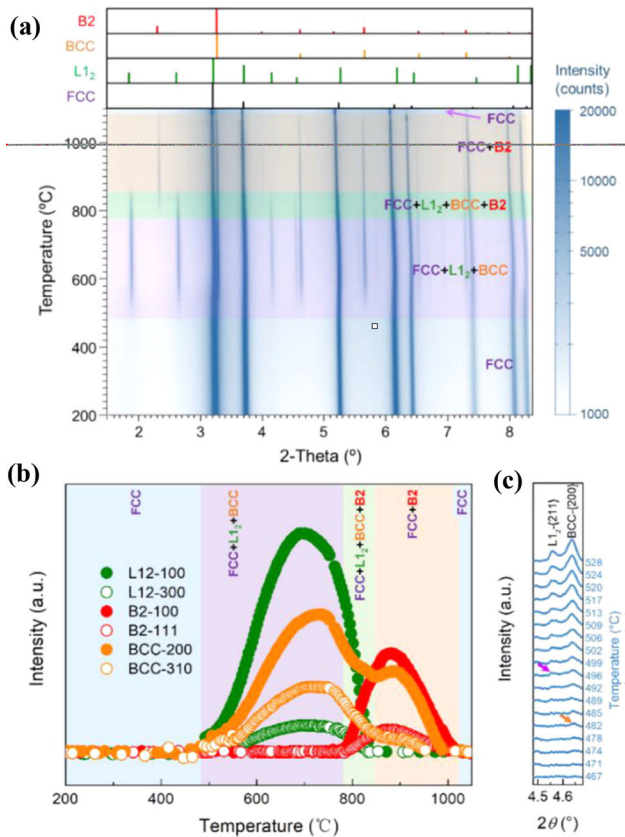


Fig. 8. (a) Phase structure evolution of the $\text{Al}_{0.5}\text{Cr}_{0.9}\text{FeNi}_{2.5}\text{V}_{0.2}$ HEAs during *in-situ* heating from 200 °C to 1100 °C. (b) Peak intensity variation with increasing temperature. (c) 1D HEXRD profiles of L1_2 and BCC phases showing that the precipitation of BCC is prior to that of L1_2 . Reprinted with permission from Ref. 34.

particle size, dislocation density, and the Burgers vector of dislocations, respectively; M is a constant depending on the effective outer cut-off radius of dislocations; C is the dislocation contrast factor.

Many researchers have performed this analysis to quantitatively explain the material's strengthening effect and strain-hardening behavior.^{8,33,47} For example, Li et al.⁸ reported a nanocrystalline nickel–cobalt solid solution with an exceptional combination of tensile strength and ductility. As shown in Fig. 9, the dislocation density ρ measured by *in situ* HEXRD increased rapidly from $7.56 \times 10^{15} \text{ m}^{-2}$ to a plateau of $1.18 \times 10^{16} \text{ m}^{-2}$ during continuous tensile loading. After reaching the peak stress, both flow stress and dislocation density remained constant, indicating that the dislocation accumulation rate in the grain interior is counterbalanced by dynamic recovery.

Using such calculation and analysis, however, one can only measure the total dislocation density, and it is still impossible to differentiate the densities of statistically stored dislocations (SSDs) and geometrically necessary dislocations (GNDs).^{25,49,50} Unfortunately, their individual contributions towards the distribution of plastic deformation are different and cannot be easily estimated without experimental

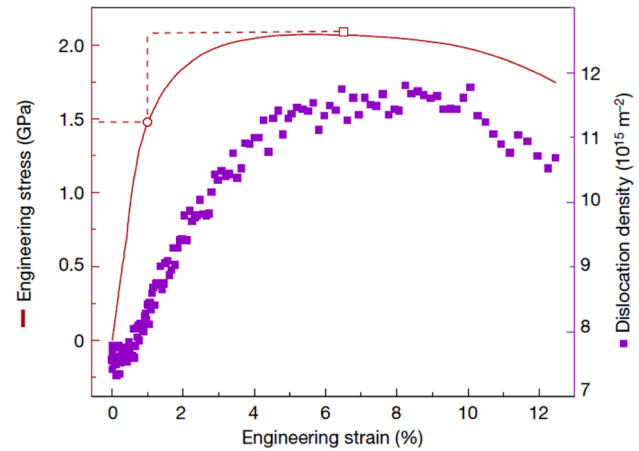


Fig. 9. Engineering stress–strain curve and corresponding dislocation density as a function of engineering strain in the nanocrystalline nickel–cobalt alloy, measured from *in-situ* HEXRD. Reprinted with permission from Ref. 8

measurement.²⁵ Actually, characterizing the evolution of GND density under straining is very important for the analysis of plastic deformation at the scale of individual grains.²⁵

CHARACTERIZING DEFORMATION MICROSTRUCTURES BY 3D MICRODIFFRACTION

Analyzing Micro-shear Banding and Local Stress Gradients

Shear banding has been extensively studied for over a century and is a ubiquitous phenomenon that occurs during the plastic deformation of many metallic materials.⁵¹ It can be regarded as heterogeneous deformation. However, the deformation process and strain evolution in the local micro-shear bands remain elusive because of their spatial–temporal complexities embedded in bulk materials. Recently, Laue x-ray microdiffraction has been applied by researchers to study dislocation microstructures and stress/strain gradients in metallic materials,^{21,25–28,49,50,52–54} both of which can help with the understanding of the heterogeneous deformation in HSMs.

Stress gradients can be quantitatively measured by Laue x-ray microdiffraction. For example, Li et al.²¹ recently managed to reveal the large stress gradients across a micro-shear band in a fatigue-deformed stainless steel. Figure 10 shows the representative results before and after tensile loading. The elastic strain of each position was represented by the $|\mathbf{q}|$ values. Overall, the primary shear band (M1) divided the grain into two parts, with the left part experiencing tensile strain but the right part compressive strain (see Fig. 10a). This indicates that complex stress/strain states may well exist in deformed microstructures. In addition, the details of the primary shear band M1 were distinguished, with lines 1 to 4 representing the wall of

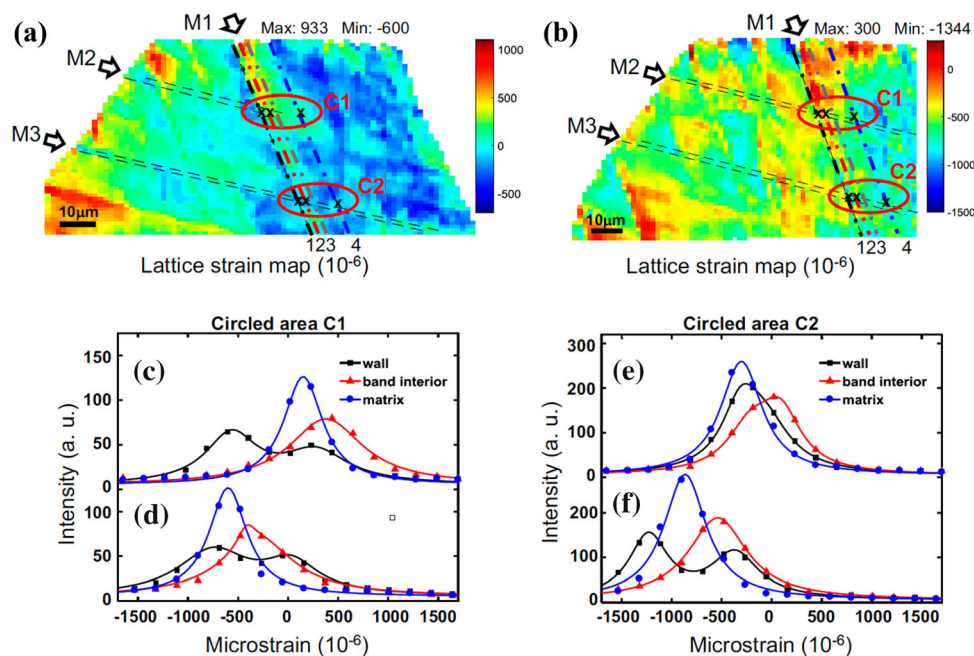


Fig. 10. (a) and (b) lattice strain distributions in the [001]//LD grain before and after applying a tensile strain of 0.5%. (c) and (d) diffraction profiles near the intersecting zone C1 before and after straining. (e) and (f) diffraction profiles near the intersecting zone C2 before and after straining. Reprinted with permission from Ref. 21, under the terms of the Creative Commons CC BY license.

M1, band interior, diffuse band wall, and grain matrix, respectively.

With high spatial resolution, the internal lattice stress in the intersection of M1 and M2/M3 (secondary micro-shear bands) was measured, as shown in Fig. 10a and b. A large strain gradient at the submicron level in the C1 area was determined, but the gradient in the C2 area was not that significant (see Fig. 10c and e). The change of micro-elastic strains in the C1 area before and after tensile loading can be shown by comparing Fig. 10c with d. The lattice strains at both the band interior and the grain matrix changed from tensile states to compressive states by tensile loading, meaning that a strong local stress interaction exists between the primary and secondary micro-shear bands. However, when comparing the C1 area with the C2 area, the change of lattice strains with loading was opposite.

Overall, these results have shown the complicated local stress states of plastic deformation in bulk materials, which have been successfully probed by Laue x-ray microdiffraction in 3D. This ability to characterize deformation microstructures at the submicron level indeed benefits analyzing heterogeneous deformation and deformation accommodation. Specifically, the technique should be an excellent tool for exploring the formation of highly dispersive strain bands in heterostructured materials. These strain bands have been extensively observed by using DIC and EBSD techniques.^{19,55} However, both nucleation and growth of the micro-strain bands, which are critical to understanding the deformation mechanisms of HSMs, are still unknown. An investigation into the formation of

these bands requires characterization techniques that enable the exploration of 3D deformed microstructures.²¹ Fortunately, Laue x-ray microdiffraction may help detect the full-field deformation gradients in HSMs.

Analyzing Geometrically Necessary Dislocations

Geometrically necessary dislocations (GNDs) are generated to maintain the continuity of the crystal lattice during plastic deformation.²⁵ Laue x-ray microdiffraction can be used to measure the local density of GNDs.^{25,26,50} Due to heterogeneous deformation in materials, the distribution of GNDs varies throughout a crystal. Thus, microdiffraction patterns often display streaked peaks. By analyzing the direction of the streaked patterns, it is feasible to measure the local density of GNDs.²⁶ For example, Ohashi et al.²⁵ measured the inhomogeneous plastic deformation in a Ni bi-crystal using Laue x-ray microdiffraction. The density of GNDs oscillates locally, giving rise to the formation of narrow slip bands at places where the GND density is high.

Laue x-ray microdiffraction is especially useful for investigating the stress gradients and distributions in heterostructured layered materials. Compared with other forms of HSMs, layered materials are more straightforward and thus more suitable for analyzing heterogeneous deformation. This is because during plastic deformation, lattice rotations, which also help accommodate the deformation,²⁵ can be more predictable and systematically controllable, thus offering a unique benefit to the

Table I. Advantages and limitations of the synchrotron techniques used for studying heterostructured materials

Techniques	Typical applications	Advantages	Limitations
High-energy x-ray diffraction	<ul style="list-style-type: none"> · Charactering structure, texture, and lattice strain · Tracking stress partitioning and phase transformations · Analyzing the overall dislocation density 	<ul style="list-style-type: none"> · In situ measurements under complex environments · High penetration for bulk samples · Large reciprocal space coverage for pair-distribution-function analysis · Fast data collection · Texture visualization 	<ul style="list-style-type: none"> · Generally revealing average structural characteristics, unless microfocus beam is used · Difficult to probe low-Z elements in materials with high-Z elements · Difficult to study materials with large grain size
Wide and small angle x-ray scattering	<ul style="list-style-type: none"> · Studying the formation of nano-precipitates/structures and voids 		
Laue x-ray microdiffraction	<ul style="list-style-type: none"> · Analyzing the local microstructures such as dislocation structures, crystal orientations, and local stress/strain gradients 	<ul style="list-style-type: none"> · High spatial resolution · The analysis of 3D deformation microstructures 	<ul style="list-style-type: none"> · Time-consuming in 3D mapping and for in situ measurements · Complex data processes under large plastic deformation

process of statistical analysis. With this advantage, the stress status and strain evolution in microstructures are more detectable and analyzable, thus benefiting the investigations into the back stress and the forward stress, together with the hetero-deformation induced (HDI) strengthening effect.⁵ Currently, microdiffraction studies have been carried out among layered materials of different kinds to investigate their deformation mechanisms.^{25,27,28,50} For example, when studying a layered aluminum with superior strength-ductility synergy, Xia et al.²⁷ analyzed the effect of the local stress and strain states by microdiffraction. However, quantitatively correlating dislocation densities to the Laue patterns is still regarded as a complex process. As a result, it is still difficult to obtain a unified model that can describe the plastic deformation of HSMs, and plenty of research needs to be performed in the future.

CURRENT CHALLENGE IN CHARACTERIZING STRAIN EVOLUTION BY SYNCHROTRON XRD

Plastic deformation and phase transformations have been widely investigated by synchrotron techniques of in situ HEXRD and Laue x-ray microdiffraction, by which the evolution of internal elastic stress and strain can be measured with a high spatial resolution. Thus, stress-induced microstructural evolution under straining and/or thermal processes is conveniently studied by the existing techniques. However, challenges in characterizing plastic deformation still exist, which has obscured our understanding of deformation physics. Though the in situ

DIC and in situ EBSD techniques can document deformation history during plastic straining,²⁰ the information obtained is limited to the surface of a sample since displacement fields and the corresponding strain maps are measured and calculated by a random pattern registered on the sample surface.

A possible solution to this challenge would be Laue x-ray microdiffraction combining monochromatic with polychromatic diffraction modes. Diffraction extracted by monochromatic x-ray microbeam can be used to map the three-dimensional strains in materials and to record the elastic strain evolution during plastic deformation, while Laue diffraction patterns obtained from the polychromatic x-ray microbeam can be used to document the change of grain or heterogeneous zone shapes, the orientation of crystals concerned, and the rotation of these crystals during deformation. With this, it is possible to gain crucial knowledge about the local deformation history in three dimensions. In addition, the correlation between GNDs and micro-strain bands is likely to be obtained, which would help understand the deformation mechanism of heterostructured materials.^{3,5} Another challenge is to characterize plastic deformation dynamically because acquiring a 3D strain distribution by the method of microdiffraction often requires a long scanning time, and thus a dynamic measurement of the 3D strain evolution is currently difficult. With increasing plastic deformation, moreover, data collection and analysis of Laue x-ray microdiffraction have become a formidable task, though some novel data-driven approaches based on machine learning algorithm have been proposed for the analysis

process.^{56,57} Efforts in this regard need to be made for a deeper understanding of deformation physics and strengthening mechanisms of heterostructured materials. Finally, a summary is given in Table I in terms of the advantages and limitations of the synchrotron-based techniques used for studying structural materials.

CONCLUSION

There is increasing evidence showing that heterostructures is an efficient design paradigm to promote salient strength-ductility enhancement. However, the deformation physics and strengthening mechanism underlying the extraordinary mechanical property are not fully understood. The advanced synchrotron-based x-ray techniques, including in situ high-energy x-ray diffraction and Laue x-ray microdiffraction, have been employed innovatively to study material's microstructures in three dimensions at a micro- or macro-scale or both. For HSMs, these techniques are effective tools for the investigation of deformation mechanisms and phase transformations. Many essential studies have been performed, including stress partitioning and plastic accommodation during tensile deformation, thermo-driven and/or stress-driven phase transformations, local stress/strain gradients and distributions, and various other deformation microstructures in heterostructured materials. Although significant progress has been made in these areas for HSMs, challenges remain regarding gaining crucial knowledge about the local deformation history. An integrated computational and experimental scheme is expected to be applied for capturing a deep understanding in deformation and design paradigms for HSMs.

ACKNOWLEDGEMENTS

This work is supported by the National Key R&D Program of China (2021YFA1200202). Y.R. also acknowledges financial support from City University of Hong Kong (project no. 9610533). Y.T.Z. acknowledges financial support of the National Science Foundation of China (51931003) and the Hong Kong Research Grants Council (GRF 11214121). XLW acknowledges the support by the Croucher Senior Research Fellowship (CityU Project Number 9509008). This research used resources of the Advanced Photon Source, a US Department of Energy (DOE) Office of Science user facility, operated for the DOE Office of Science by Argonne National Laboratory under Contract No. DE-AC02-06CH11357. XLW acknowledges the support by the Croucher Senior Research Fellowship (CityU Project Number 9509008).

CONFLICT OF INTEREST

The authors declare that they have no conflict of interest.

REFERENCES

1. S.S. Sohn, K. Choi, J.-H. Kwak, N.J. Kim, and S. Lee, *Acta Mater.* 78, 181 (2014).
2. I.A. Ovid'ko, R.Z. Valiev, and Y.T. Zhu, *Prog. Mater. Sci.* 94, 462 (2018).
3. Y. Zhu and X. Wu, *Prog. Mater. Sci.* 131, 101019 (2023).
4. X. Wu, M. Yang, F. Yuan, G. Wu, Y. Wei, X. Huang, and Y. Zhu, *Proc. Natl. Acad. Sci. U. S. A.* 112, 14501 (2015).
5. Y. Zhu, K. Ameyama, P.M. Anderson, I.J. Beyerlein, H. Gao, H.S. Kim, E. Lavernia, S. Mathaudhu, H. Mughrabi, R.O. Ritchie, N. Tsuji, X. Zhang, and X. Wu, *Mater. Res. Lett.* 9, 1 (2020).
6. X.T. Fang, G.Z. He, C. Zheng, X.L. Ma, D. Kaoumi, Y.S. Li, and Y.T. Zhu, *Acta Mater.* 186, 644 (2020).
7. C.X. Huang, Y.F. Wang, X.L. Ma, S. Yin, H.W. Höppel, M. Göken, X.L. Wu, H.J. Gao, and Y.T. Zhu, *Mater. Today* 21, 713 (2018).
8. H. Li, H. Zong, S. Li, S. Jin, Y. Chen, M.J. Cabral, B. Chen, Q. Huang, Y. Chen, Y. Ren, K. Yu, S. Han, X. Ding, G. Sha, J. Lian, X. Liao, E. Ma, and J. Sun, *Nature* 604, 273 (2022).
9. R. Cao, Q. Yu, J. Pan, Y. Lin, A. Sweet, Y. Li, and R.O. Ritchie, *Mater. Today* 32, 94–107 (2020).
10. P. Shi, R. Li, Y. Li, Y. Wen, Y. Zhong, W. Ren, Z. Shen, T. Zheng, J. Peng, X. Liang, P. Hu, N. Min, Y. Zhang, Y. Ren, P.K. Liaw, D. Raabe, and Y.D. Wang, *Science* 373, 912 (2021).
11. P. Shi, W. Ren, T. Zheng, Z. Ren, X. Hou, J. Peng, P. Hu, Y. Gao, Y. Zhong, and P.K. Liaw, *Nat. Commun.* 10, 489 (2019).
12. J.T. Avallone, T.J. Nizolek, B.B. Bales, and T.M. Pollock, *Acta Mater.* 176, 189–198 (2019).
13. V.E. Gromov, Y.F. Ivanov, O.A. Stolboushkina, and S.V. Kononov, *Mater. Sci. Eng. A* 527, 858–861 (2010).
14. D. Jiang, J. Song, H. Yang, Y. Liu, X. Jiang, Y. Ren, K. Yu, and L. Cui, *Compos. B Eng.* 202, 108403 (2020).
15. D. Salas, Y. Wang, T.C. Duong, V. Attari, Y. Ren, Y. Chumlyakov, R. Arróyave, and I. Karaman, *Acta Mater.* 206, 116616 (2021).
16. Y.C. Wang, A. Misra, and R.G. Hoagland, *Scr. Mater.* 54, 1593–1598 (2006).
17. Y.B. Lei, Z.B. Wang, J.L. Xu, and K. Lu, *Acta Mater.* 168, 133–142 (2019).
18. X. Wu, M. Yang, R. Li, P. Jiang, F. Yuan, Y. Wang, Y. Zhu, and Y. Wei, *Sci. China Mater.* 64, 1534 (2021).
19. Y. Wang, C. Huang, Y. Li, F. Guo, Q. He, M. Wang, X. Wu, R.O. Scattergood, and Y. Zhu, *Int. J. Plast.* 124, 186 (2020).
20. D. Yan, C.C. Tasan, and D. Raabe, *Acta Mater.* 96, 399 (2015).
21. R. Li, Q. Xie, Y.D. Wang, W. Liu, M. Wang, G. Wu, X. Li, M. Zhang, Z. Lu, C. Geng, and T. Zhu, *Proc. Natl. Acad. Sci. U. S. A.* 115, 483 (2018).
22. L. Wang, M. Li, and J. Almer, *Acta Mater.* 62, 239 (2014).
23. M.L. Young, J.D. Almer, M.R. Daymond, D.R. Haefner, and D.C. Dunand, *Acta Mater.* 55, 1999 (2007).
24. K. Chatterjee, J.Y.P. Ko, J.T. Weiss, H.T. Philipp, J. Becker, P. Purohit, S.M. Gruner, and A.J. Beaudoin, *J. Mech. Phys. Solid* 109, 95 (2017).
25. T. Ohashi, R.I. Barabash, J.W.L. Pang, G.E. Ice, and O.M. Barabash, *Int. J. Plast.* 25, 920 (2009).
26. L. Wang, R. Barabash, T. Bieler, W. Liu, and P. Eisenlohr, *Metall. Mater. Trans. A* 44, 3664 (2013).
27. Y. Xia, K. Miao, H. Wu, L. Geng, C. Xu, C.-S. Ku, and G. Fan, *Int. J. Plast.* 152, 103240 (2022).
28. T. Yu, Y. Du, G. Fan, R. Xu, R. Barabash, N. Hansen, X. Huang, and Y. Zhang, *Acta Mater.* 202, 149 (2021).
29. Z.H. Cong, N. Jia, X. Sun, Y. Ren, J. Almer, and Y.D. Wang, *Metall. Mater. Trans. A* 40, 1383 (2009).
30. B. Feng, X. Kong, S. Hao, Y. Liu, Y. Yang, H. Yang, F. Guo, D. Jiang, T. Wang, Y. Ren, and L. Cui, *Acta Mater.* 194, 565 (2020).
31. X. Rao, Y. Ru, F. Guo, Y. Ren, L. Cui, and K. Yu, *Scr. Mater.* 220, 114942 (2022).

32. X. Zhang, M.D. McMurtrey, L. Wang, R.C. O'Brien, C.-H. Shiao, Y. Wang, R. Scott, Y. Ren, and C. Sun, *Jom-U*s 72, 4167 (2020).
33. X. Fang, Q. Xue, K. Yu, R. Li, D. Jiang, L. Ge, Y. Ren, C. Chen, and X. Wu, *Mater. Res. Lett.* 8, 417 (2020).
34. L. Wang, L. Wang, S. Zhou, Q. Xiao, Y. Xiao, X. Wang, T. Cao, Y. Ren, Y.-J. Liang, L. Wang, and Y. Xue, *Acta Mater.* 216, 117121 (2021).
35. P. Hou, Y. Li, W. Zhang, D. Chae, J.-S. Park, Y. Ren, Y. Gao, and H. Choo, *Materialia* 18, 101162 (2021).
36. D. Zhang, L. Wang, H. Zhang, A. Maldar, G. Zhu, W. Chen, J.-S. Park, J. Wang, and X. Zeng, *Acta Mater.* 189, 93 (2020).
37. O. Muránsky, L. Balogh, M. Tran, C.J. Hamelin, J.S. Park, and M.R. Daymond, *Acta Mater.* 175, 297 (2019).
38. R. Li, Y. Wang, N. Xu, Z. Yan, S. Li, M. Zhang, J. Almer, Y. Ren, and Y.-D. Wang, *Acta Mater.* 229, 117810 (2022).
39. Y. Ren, *Jom-U*s 64, 140 (2012).
40. Y. Ren and X. Zuo, *Small Methods* 2, 1800064 (2018).
41. M. Li, L. Wang, and J.D. Almer, *Acta Mater.* 76, 381 (2014).
42. B.C. Larson, W. Yang, G.E. Ice, J.D. Budai, and J.Z. Tischler, *Nature* 415, 887 (2002).
43. W. Liu and G.E. Ice, *Strain and Dislocation Gradients From Diffraction: Spatially-Resolved Local Structure and Defects*, ed. R.I. Barabash and G.E. Ice (Imperial College Press, London, 2014), p. 53–81.
44. Y. Wang, Y. Wei, Z. Zhao, Z. Lin, F. Guo, Q. Cheng, C. Huang, and Y. Zhu, *Scripta Mater.* 207, 114310 (2022).
45. J. Almer, U. Lienert, R.L. Peng, C. Schlauer, and M. Oden, *J. Appl. Phys.* 94, 697 (2003).
46. Y. Zhang, T.T. Zuo, Z. Tang, M.C. Gao, K.A. Dahmen, P.K. Liaw, and Z.P. Lu, *Prog. Mater. Sci.* 61, 1 (2014).
47. T. Ungar, *Mater. Sci. Eng. A* 309, 14 (2001).
48. T. Ungár and A. Borbély, *Appl. Phys. Lett.* 69, 3173 (1996).
49. L. Wang, R.I. Barabash, Y. Yang, T.R. Bieler, M.A. Crimp, P. Eisenlohr, W. Liu, and G.E. Ice, *Metall. Mater. Trans. A* 42, 626 (2010).
50. R.I. Barabash, O.M. Barabash, M. Ojima, Z. Yu, J. Inoue, S. Nambu, T. Koseki, R. Xu, and Z. Feng, *Metall. Mater. Trans. A* 45, 98 (2013).
51. S.D. Antolovich and R.W. Armstrong, *Prog. Mater. Sci.* 59, 1 (2014).
52. H. Chen, Y.D. Wang, Z. Nie, R. Li, D. Cong, W. Liu, F. Ye, Y. Liu, P. Cao, F. Tian, X. Shen, R. Yu, L. Vitos, M. Zhang, S. Li, X. Zhang, H. Zheng, J.F. Mitchell, and Y. Ren, *Nat. Mater.* 19, 712 (2020).
53. D. Li, G. Fan, X. Huang, D. Juul Jensen, K. Miao, C. Xu, L. Geng, Y. Zhang, and T. Yu, *Acta Mater.* 206, 116627 (2021).
54. R.I. Barabash, G.E. Ice, M. Kumar, J. Ilavsky, and J. Belak, *Int. J. Plast.* 25, 2081 (2009).
55. Y. Wang, Y. Wei, Z. Zhao, H. Long, Z. Lin, F. Guo, Q. He, C. Huang, and Y. Zhu, *Int. J. Plast.* 149, 103159 (2022).
56. Y. Song, N. Tamura, C. Zhang, M. Karami, and X. Chen, *Acta Crystallogr. A Found Adv.* 75, 876–888 (2019).
57. G.N. Zhou, J.W. Kou, Y. Li, W.X. Zhu, K. Chen, and N. Tamura, *Quantum Beam Sci.* 2, 13 (2018).

Publisher's Note Springer Nature remains neutral with regard to jurisdictional claims in published maps and institutional affiliations.

Springer Nature or its licensor (e.g. a society or other partner) holds exclusive rights to this article under a publishing agreement with the author(s) or other rightsholder(s); author self-archiving of the accepted manuscript version of this article is solely governed by the terms of such publishing agreement and applicable law.